Tunable Strong Coupling of Mechanical Resonance between Spatially Separated $FePS_3$ Nanodrums

Šiškins, Makars; Sokolovskaya, Ekaterina; Lee, Martin; Mañas-Valero, Samuel; Davidovikj, Dejan; Van Der Zant, Herre S.J.; Steeneken, Peter G.

DOI
10.1021/acs.nanolett.1c03010

Publication date
2021

Document Version
Final published version

Published in
Nano Letters

NANO LETTERS

pubs.acs.org/NanoLett

Letter

Tunable Strong Coupling of Mechanical Resonance between Spatially Separated $FePS_3$ Nanodrums

Makars Šiškins,*[,‖] Ekaterina Sokolovskaya,[‖] Martin Lee, Samuel Mañas-Valero, Dejan Davidovikj, Herre S. J. van der Zant, and Peter G. Steeneken*

Cite This: https://doi.org/10.1021/acs.nanolett.1c03010

Read Online

ACCESS | Metrics & More | Article Recommendations | Supporting Information

ABSTRACT: Coupled nanomechanical resonators made of two-dimensional materials are promising for processing information with mechanical modes. However, the challenge for these systems is to control the coupling. Here, we demonstrate strong coupling of motion between two suspended membranes of the magnetic 2D material $FePS_3$. We describe a tunable electromechanical mechanism for control over both the resonance frequency and the coupling strength using a gate voltage electrode under each membrane. We show that the coupling can be utilized for transferring data between drums by amplitude modulation. Finally, we also study the temperature dependence of the coupling and how it is affected by the antiferromagnetic phase transition characteristic of this material. The presented electrical coupling of resonant magnetic 2D membranes holds the promise of transferring mechanical energy over a distance at low electrical power, thus enabling novel data readout and information processing technologies.

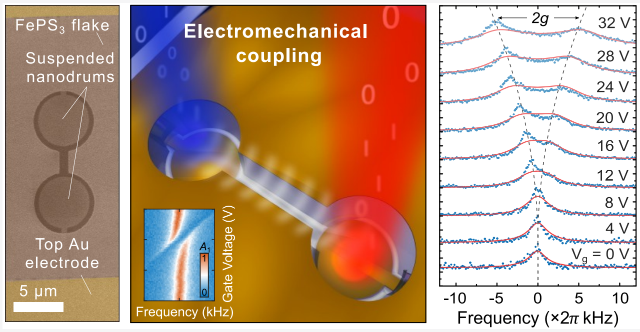

KEYWORDS: *Two-dimensional materials, Membranes, Coupling, Resonance structures, Oscillation, Magnetic properties*

■ INTRODUCTION

Nanoelectromechanical systems (NEMS) are attracting the attention of the scientific community for their potential to study novel quantum and electromagnetic effects at the nanoscale.[1−3] Along with that, micro- and nanoresonators have been studied for various applications, including sensitive mass detection,[4,5] band-pass filters with variable properties,[6] logic gates,[7−9] and signal amplifiers.[10] For instance, arrays of coupled highly cooperative NEMS and oscillators are already utilized for the coherent manipulation of phonon populations[11−13] and for data processing and storage.[3,14] Recently, NEMS made out of two-dimensional (2D) materials have also gained interest due to the prospect of realizing high-performance oscillators[15,16] and novel sensor concepts.[17] This is not only due to the atomic thinness of these devices but also because the fabrication methodology allows the integration of a range of materials and their heterostructures, with a wide range of magnetic, optical, and electrical properties, on the same chip.[18] Hence, coupling NEMS resonators made of 2D materials and heterostructures promises even more interesting implementation possibilities.

Various studies have reported mechanical coupling between different resonance modes of the same 2D membrane by mechanical, optical, and electronic means.[19−22] However, the realization of coupling between resonances of spatially separated 2D membranes has appeared to be more difficult and was only recently achieved via a mechanical phononic transduction mechanism.[23,24] A mechanically mediated coupling mechanism via a phonon bath was demonstrated,[23,24] but although the coupling could be adjusted via the individual resonance frequencies of the resonators, the coupling strength itself is fixed by the mechanical geometry of the structure that determined the phonon bath. In order to achieve full control over the coupling, a tunable transduction mechanism is needed that not only adjusts the degree of coupling between the resonators but also regulates their resonance frequencies.

Here, we demonstrate an electrical transduction mechanism for coupling mechanical resonances of two spatially separated membranes made of a van der Waals material, allowing control over both the resonance frequency and the coupling strength via gate electrodes. We use the mechanism to strongly couple the fundamental mechanical modes of two suspended circular antiferromagnetic $FePS_3$ membranes that are separated by an edge-to-edge distance of 2 μm. We show that the coupling mechanism can be utilized for transferring data from one drum

Received: August 4, 2021
Revised: December 3, 2021

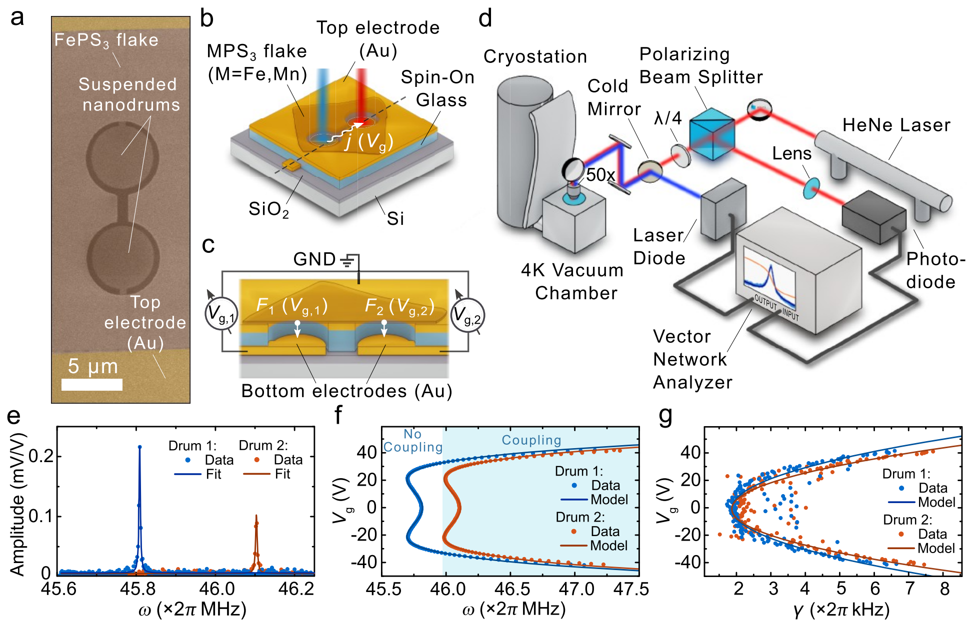

Figure 1. Measurement principle and setup. (a) False-color SEM image of the sample. Flake thickness: 25.6 ± 0.4 nm. (b) Schematics of the device and optical measurement principle. $j(V_g)$ is the voltage-dependent coupling parameter. (c) Schematics of a cross-section of the device, electrically induced force $F_{1,2}$, and gate voltage V_g. (d) Laser interferometry setup: red laser, λ_{red} = 632 nm; blue laser, λ_{blue} = 405 nm. (e) Detected resonance peaks for the two suspended drums at T = 4 K: filled dots, measured data; solid lines, linear harmonic oscillator fits. (f) Resonance frequencies $\omega(V_g)$ of drums 1 and 2, extracted from fits similar to that in (e): filled dots, measured data; solid line, continuum mechanics model[30,31] (see section SI 1). The blue region indicates the parameter space where the $\omega_1 = \omega_2$ condition can be met. (g) Dissipation rate $\gamma(V_g)$ for two drums extracted from fits similar to those shown in (e): filled dots, measured data; solid lines, Joule dissipation model[32−34] (see section SI 2).

to the other, a feature that is useful in data processing and storage systems. Coupling of magnetic materials such as $FePS_3$ is of interest, since their mechanical resonances can be sensitive to both the magnetic phase[25] and the magnetization of that phase.[26] To investigate this, we study the temperature dependence of the coupling strength and in particular how it is affected by the antiferromagnetic phase transition at the Néel temperature, $T_N \approx 114$ K.[27,28]

RESULTS AND DISCUSSION

Laser Interferometry of $FePS_3$ Resonators. We have fabricated two circular suspended $FePS_3$ resonators on top of a Si/SiO_2 substrate on which we define an array of Au bottom gate electrodes. A layer of spin-on glass (SOG)[29] is used to electrically insulate the bottom electrodes from the top electrode, as indicated in Figure 1 (see also Methods in the Supporting Information). Then, two spatially separated circular cavities of r = 3 μm in radius are etched in the SOG/Au top layer,[29] such that the local circular gate electrode with a radius of r_g = 2.5 μm is located at the bottom of the cavity. We transfer a flake of few-layer $FePS_3$ exfoliated from a synthetically grown bulk crystal[25] over these cavities by a dry transfer technique (see Methods in the Supporting Information) to create two separated circular membranes of the same flake, as depicted in Figure 1a−c. As shown in Figure 1b, we focus red and blue lasers on these drums to excite the motion of one membrane and measure the displacement of the other using a laser interferometry technique (see Methods in the Supporting Information), thus probing the coupling between fundamental vibration modes of these membranes. To realize the study as a function of gate voltage and the corresponding electrostatically induced strain for both drums, we use local electrodes that allow us to individually adjust the gate voltage, V_g, for each of the resonators (see Figure 1c). The single $FePS_3$ flake, out of which the resonators are formed, is contacted via a top metal electrode to ground. A false-color scanning electron microscopy (SEM) image in Figure 1a shows a 25.6 ± 0.4 nm $FePS_3$ flake suspended over the electrodes forming two separated membrane resonators. The resonators are placed in a dry cryostat with optical access that is connected to a laser interferometry setup, as shown in Figure 1d (see Methods in the Supporting Information).

When operating the laser interferomery technique with both lasers focused at the same position on the same membrane, we independently characterize the resonance spectra of the fundamental membrane modes of drums 1 and 2 at a temperature of 4 K, as shown in Figure 1e. We fit these spectra to a harmonic oscillator model and extract the resonance frequencies $\omega_{1,2}$ as a function of V_g, which are displayed with filled blue and orange dots in Figure 1f. The resonances $\omega_{1,2}(V_g)$ of both drums closely follow the continuum mechanics model,[30,31] as shown by the solid blue and orange lines in Figure 1f (see section SI 1). At certain values of $V_{g,1}$ and $V_{g,2}$, the frequencies ω_1 and ω_2 of the corresponding resonance peaks match at $\omega_1 = \omega_2$, as indicated by the light blue region in Figure 1f. In this regime we can expect an avoided frequency crossing if the exchange of the excitation energy between the drums is sufficiently large and the drums are strongly coupled.[3] The coupling strength is also related to the dissipation $\frac{1}{Q_{1,2}}$ of the resonators involved.[11,19] Hence, we plot the corresponding mechanical energy dissipation rates $\gamma_{1,2} = \frac{\omega_{1,2}}{Q_{1,2}}$ of the $FePS_3$ membranes in Figure 1g. Measured $\gamma_{1,2}(V_g)$ values follow a parabolic behavior, in accordance with a Joule dissipation model (solid blue and orange lines; see section SI 2), which can be attributed to

https://doi.org/10.1021/acs.nanolett.1c03010
Nano Lett. XXXX, XXX, XXX−XXX

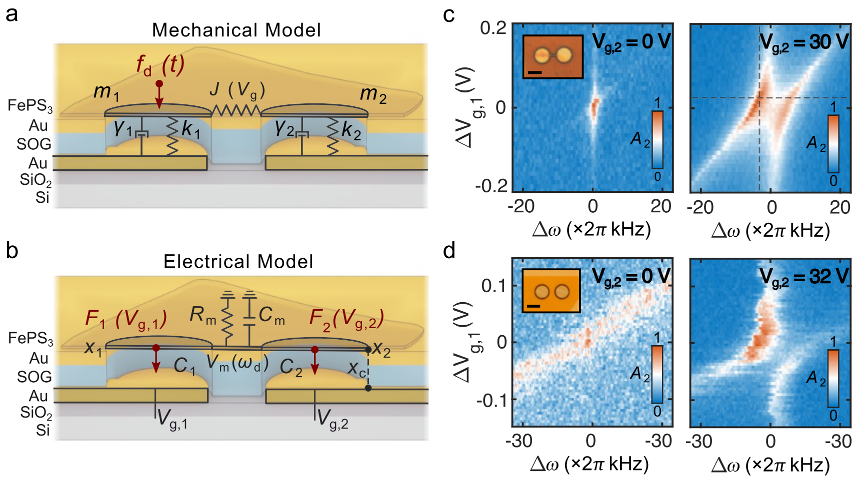

Figure 2. Strong coupling of spatially separated $FePS_3$ membrane resonators at T = 4 K. Schematics of coupled membrane oscillators. (a) Mechanical model: $m_{1,2}$ is the effective mass, $k_{1,2}$ the effective stiffness, and $J(V_g)$ the gate voltage dependent coupling parameter. (b) Electrical model: $C_{1,2}$ is the capacitance of each drum toward the gate electrode that is kept at a voltage V_g, R_m the interface resistance between the flake and the underlying ground electrode, C_m the capacitance to ground, and $V_m(\omega_d)$ the voltage between the membranes. (c) Sample with a suspended channel between the drums: (left) weak coupling of motion between spatially separated drums at $V_{g,1}$ = 36.9 V and $V_{g,2}$ = 0 V and $\Delta\omega = \omega_d - \omega_2$; (inset) optical image of the sample, with a thickness of 25.6 ± 0.4 nm (scale bar 6 μm); (right) strong coupling of motion between spatially separated drums at $V_{g,1}$ = 37.2 V and $V_{g,2}$ = 30 V. (d) Sample without a suspended channel between the drums (see section SI 7): (left) weak coupling of motion at $V_{g,1}$ = 32.4 V and $V_{g,2}$ = 0 V; (inset) optical image of the sample with a thickness of 14.5 ± 0.3 nm (scale bar 6 μm); (right) strong coupling of motion at $V_{g,1}$ = 34.5 V and $V_{g,2}$ = 32 V.

capacitive displacement currents in the suspended region of the flake.[32−34]

Electromechanical Coupling Model. The mechanical behavior of coupled membrane resonators can be modeled by two coupled resonators, schematically depicted in Figure 2a. The motion of coupled resonators is described by

$$\begin{cases} \ddot{x}_1 + \gamma_1\dot{x}_1 + \omega_1^2 x_1 = jx_2 + f_d \cos \omega_d t \\ \ddot{x}_2 + \gamma_2\dot{x}_2 + \omega_2^2 x_2 = jx_1 \end{cases} \tag{1}$$

where $x_{1,2}$ are the membrane displacements and f_d is the force at a drive frequency ω_d. The coupling parameter $j = \frac{J}{\sqrt{m_1 m_2}}$, where $m_{1,2}$ is the effective mass, is responsible for the transfer of energy between the two resonators and thus coupling of the mechanical motion. Several coupling mechanisms can contribute to J (see section SI 3). In this work, we present evidence for an electromechanical coupling mechanism for adjusting the coupling strength between two 2D material resonators.

Figure 2b shows a schematic of the electrical circuit that mediates the coupling (see section SI 4). The suspended part of the thin $FePS_3$ flake, which covers the two cavities, is both resistively and capacitively connected to ground via the interface between the flake and the Au top electrode. We assume that the voltage $V_{m,DC}$ that is established between drum 1 and drum 2 is zero since the Au top electrode effectively shunts potential differences between the drums. However, since the capacitance C_m between the $FePS_3$ flake and Au top electrode is large, it dominates the electrical coupling of the flake to ground ($\frac{1}{\omega_d C_m} \ll R_m$, where R_m is the resistance to ground). As is outlined in section SI 4, the optothermal drive of the first drum at nonzero $V_{g,1}$ then results in a nonzero flake voltage $V_{m,AC}$ that causes an electrostatic force on the second drum, $F_{2,AC} = -J_{el}x_{10} \sin(\omega_d t)$, where x_{10} is the amplitude of periodic displacement and the electrical coupling parameter J_{el} is given by

$$J_{el} \cong \frac{(\varepsilon_0 \pi r_g^2)^2}{C_m} \frac{V_{g,1}V_{g,2}}{(x_c - x_{g,1})^2(x_c - x_{g,2})^2} \tag{2}$$

where ε_0 is the dielectric permittivity of vacuum, $x_g(V_g)$ the static deflection at the center of membrane (see section SI 1), and x_c the separation between the membrane and the bottom electrode. When eqs 1 and 2 are combined, it is seen that J_{el} results in a transfer of mechanical energy via electromechanical coupling between the spatially separated $FePS_3$ drums. It is notable that the driving force on the second drum $F_{2,AC}$ is proportional to the product of the individual gate voltages applied to each of the drums, which originates from the quadratic dependence of electrostatic force with respect to total voltage. This means that at V_g = 0 V on either drum, the electrical coupling parameter J_{el} = 0 even if $\omega_1 = \omega_2$ and $f_d > 0$. This property distinguishes the expected behavior of this mechanism from phonon- or tension-mediated coupling,[19,21,23,24] where frequency matching and a nonzero driving force acting on one of the drums are sufficient conditions for coupling and thus splitting of the resonance frequency to occur.

We use this characteristic to provide evidence for the proposed mechanism, by first matching the resonance frequencies of the drums by tuning $\omega_{1,2}$ such that $\omega_1 = \omega_2$ using electrostatic pulling, as shown in Figure 1f. Then we alter $V_{g,1}$ of the drum that we drive with the modulated blue laser, while measuring the amplitude of motion of the other drum that is probed with the red laser at a constant $V_{g,2}$. Figure 2c shows the resonance peak splitting for different V_g values applied to both membranes. Two distinct regimes are visible: one that corresponds to weak coupling at $V_{g,2}$ = 0 V (and J_{el} = 0) and another that corresponds to strong coupling with the avoided frequency crossing visible at $V_{g,2}$ = 30 V (and $J_{el} \neq 0$). We did not observe any change to the avoided crossing related

https://doi.org/10.1021/acs.nanolett.1c03010
Nano Lett. XXXX, XXX, XXX−XXX

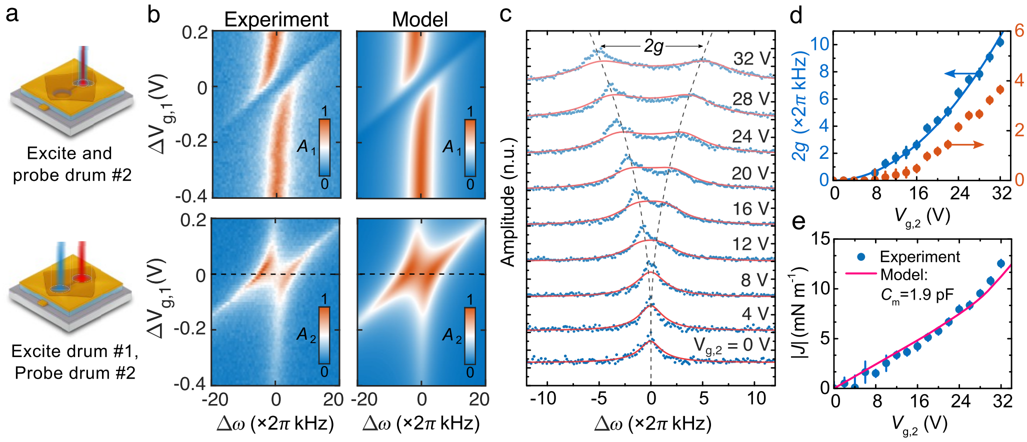

Figure 3. Comparison between the coupled oscillators model and experiments at $T = 4$ K. (a) Schematic indication of the position of lasers for each row of data in (b). (b) Measured normalized amplitudes $A_{1,2}$ of the resonance peaks at $V_{g,1} = 37.2$ V and $V_{g,2} = 30$ V compared with the model of eqs 1 and 2 (see sections SI 1−SI 4). The dashed horizontal line shows the extraction of data given in (c) at $\Delta\omega = \omega_d - \omega_2$. (c) Amplitude A_2 of the resonance peak splitting of drum 2 at different $V_{g,2}$ values: filled blue dots, measured data; solid red lines, fit to the model of eq 3; dashed black line, positions of peak maxima used to extract $2g$. (d) Splitting $2g$ and cooperativity plotted against V_g: filled blue dots, measured $2g$ obtained from (c); solid blue line, fit to a parabola used as a guide to the eye; filled orange dots, cooperativity calculated from $2g$ and the corresponding $\gamma_{1,2}$ values from Figure 1g. (e) Measured and modeled coupling constant $J(V_g)$: filled blue dots, J extracted from the fit in (c); solid magenta line, comparison to the model of eq 2. Error bars in (d) and (e) are indicated with vertical colored lines.

to the change of laser intensity or its modulation amplitude (see section SI 5). Also, resonance peaks disappear when the blue laser drive is focused on the unsuspended region of $FePS_3$ (see section SI 6). The observed strong coupling between the drums, and its gate voltage dependence, can therefore not be attributed to periodic heating from the laser beam or to other parasitic electrical actuation mechanisms. Moreover, we observed the same behavior in a test sample without a suspended channel connecting the two membranes, as shown in Figure 2d (see section SI 7), thus providing additional evidence ruling out the possibility of strong tension-mediated direct mechanical coupling. We note that the nonzero amplitudes in the weak coupling regime at $V_{g,2} = 0$ V in Figure 2c,d indicate the presence of some other, much less pronounced, mechanisms of weak coupling (see section SI 3). However, the evidence above suggests that the contribution of these mechanisms, which can couple the motion of two spatially separated $FePS_3$ resonators under our experimental conditions, is negligible in comparison to the dominant mechanism that we propose in Figure 2b and eq 2 with $J \approx J_{el}$.

Strong Coupling between Spatially Separated Nanodrums. We now study the coupling mechanism in more detail by comparing the two laser configurations using the setup described above, in which we either focus red and blue lasers on separate drums to excite one membrane and measure the motion of the other or focus them on the same drum to excite and measure a single drum (see Figure 3a). We apply the corresponding V_g to the drums in order to match their $\omega_{1,2}$ values and measure the avoided crossing of the resonance frequencies in both configurations of lasers. By solving eq 1, we find amplitudes for the two configurations of lasers as[35]

$$A_1 = \frac{f_d}{\gamma_1 \omega_d} \frac{\sqrt{\delta_2^2 + 1}}{\Delta}$$
$$A_2 = \frac{f_d}{\gamma_1 \gamma_2 \omega_d^2} \frac{|j|}{\Delta} \qquad (3)$$

where A_1 is the oscillation amplitude with lasers on the same drum, A_2 the amplitude with lasers on different drums, $\Delta = \sqrt{(\Lambda + 1 - \delta_1\delta_2)^2 + (\delta_1 + \delta_2)^2}$ the coupling strength coefficient, and $\delta_{1,2} = \frac{\omega_{1,2}^2 - \omega_d^2}{\gamma_{1,2}\omega_d}$ the detuning. In Figure 3b the measured amplitudes $A_{1,2}$ at $V_{g,2} = 30$ V are compared to simulations based on the continuum mechanics model (see section SI 1) as well as eqs 1 and 2. The model is in good agreement with the experimental data (see sections SI 1−SI 4).

We now investigate the gate voltage dependence of strong coupling between the separated $FePS_3$ membrane resonators. In Figure 3c we show the resonance peak splitting $2g$ with increasing $V_{g,2}$. We extract $2g$ from peak maxima of the measured data in Figure 3c, which we plot together with the cooperativity calculated[19,23] as $\frac{(2g)^2}{\gamma_1\gamma_2}$. A strong coupling regime and an avoided crossing is reached when the figure of merit of the coupling, the cooperativity, is above 1, which is achieved for $V_{g,2} > 16$ V. We also fit A_2 of the same data set in Figure 3c to eq 3 to extract j. Figure 3e displays the measured coupling constant $J(V_g)$ (filled blue dots), in comparison to the electrical coupling model of eq 2 (solid magenta line). The model follows the experiment closely for $C_m = 1.9$ pF (as supported by finite element method simulations; see section SI 8), reproducing both the quasi-linear part of the data at $V_{g,2} < 24$ V and the nonlinear part at $V_{g,2} > 24$ V that appears due to the deflection of the membrane x_g at larger V_g. This result is also reproducible for different samples (see section SI 9).

Amplitude-Modulated Transmission of Information. In the strong coupling regime the excitation energy is transferred between the resonators. In Figure 4 we demonstrate that this channel of energy exchange can be amplitude-modulated to transfer binary data from one drum to another. We lock the gate voltage V_g of both drums and lock the excitation frequency at ω_d, as indicated with dashed lines in Figure 2c. Then, we modulate the drive power of the blue laser between 2.5 and 5 dBm with a step function and thus the amplitude of excitation force f_d of drum 1, while measuring the

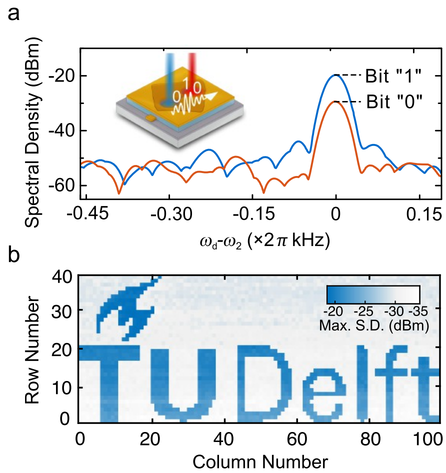

Figure 4. Information transfer between drums at T = 4 K. (a) Measured spectral density near ω_2 at 0 and 1 bit of amplitude-modulated excitation. Inset: schematics of the experiment. (b) Map of the maximum of the spectral density showing a binary picture that was sent to drum 1 and received at drum 2 at a bit rate of 4 bits/s.

motion of drum 2 using the red laser. The peak value in the measured spectral density corresponds to the resonant motion of drum 2 at the excitation frequency ω_d, as shown in Figure 4a. The lower maximum of the measured spectral peak density corresponds to a bit with a value of 0, while the larger maximum corresponds to a bit with a value of 1. Using this approach, we send a binary image to drum 1 and read it out on drum 2 (see section SI 10). The result is plotted in Figure 4b as a map of the maximum spectral density of the detected resonance peak on drum 2. The received picture is clearly distinguishable with no bits lost during the transfer.

Coupling near the Antiferromagnetic Néel Temperature. $FePS_3$ is an antiferromagnetic semiconductor at low temperature[36,37] with a Néel temperature $T_N \approx 114$ K,[27,28] where it exhibits a phase transition to a paramagnetic phase. The phase change in $FePS_3$ is accompanied by a large anomaly in the thermal expansion coefficient that produces an accumulation of substantial tensile strain in the membrane[25] as it is cooled from room temperature to 4 K. As a consequence, at cryogenic temperatures membranes of $FePS_3$, even those tens of nanometers thick,[25] have large quality factors of $(2-6) \times 10^4$ that are comparable to those of high-Q membranes made of strained monolayers of WSe_2 and $MoSe_2$.[34] In earlier works it was shown that the mechanical resonances of magnetic membranes can be sensitive to both the magnetic phase[25] and the magnetization of that phase.[26] Therefore, when the membranes are strongly coupled, small differences in magnetization can result in large differences in the resonance frequencies and the mechanical damping of the membranes and thus the coupling strength, making such coupled resonators very sensitive to small changes in the magnetic state of the material.

In Figure 5a–d, we study a sample of $FePS_3$ to assess the temperature dependence of the coupling strength near the T_N value. Following the experimental organization and analysis from above, we fix $V_{g,2}$ of the drum 2 at 29 V and measure the resonance frequency, coupling parameter, and cooperativity as a function of temperature. As shown in Figure 5a, when the sample is heated from 4 to 135 K, $\omega_{1,2}$ values soften near the T_N value of 107 K. This also appears as a characteristic peak in $\frac{d(f_0^2)}{dT} = \frac{1}{4\pi^2}\frac{d(\omega_2^2)}{dT}$ in Figure 5c and originates from the anomaly in the specific heat of the material at T_N.[25,27] Interestingly, with the temperature approaching T_N, the splitting of the resonance peak disappears, as shown in Figure 5b. However, as follows from eq 2, J_{el} is not expected to have a strong temperature dependence or abruptly drop to zero near T_N, which is also notable from Figure 5c, where we plot the experimentally obtained $J(T)$ value. Instead, this switch from a strong to weak coupling regime is related to a continuous decrease of the cooperativity due to increasing $\gamma_{1,2}$ values as it approaches the transition temperature, as shown in Figure 5d. This behavior of

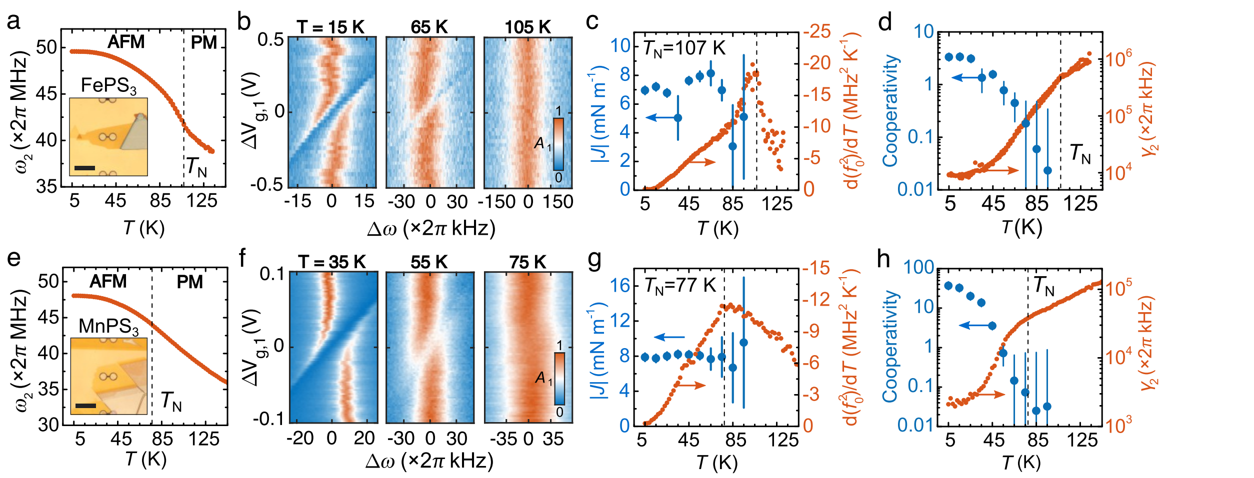

Figure 5. Temperature dependence of the coupling between antiferromagnetic membranes. (a) Resonance frequency ω_2 of the $FePS_3$ drum as a function of temperature. Inset: optical image of the $FePS_3$ sample with a thickness of 13.9 ± 0.3 nm (scale bar 18 μm). (b) Normalized amplitude A_1 of the resonance peak splitting at $\Delta\omega = \omega_d - \omega_2$ plotted for three different temperatures. (c) Filled blue dots indicate the measured coupling constant J, filled orange dots indicate the $\frac{d(f_0^2)}{dT}$ value of the data in (a). (d) Filled blue dots indicate the cooperativity, and filled orange dots indicate the dissipation rate γ_2. (e–h) follow the same structure as the (a–d) with the data shown for a $MnPS_3$ sample. Inset of (e): Optical image of the $MnPS_3$ sample with a thickness of 10.5 ± 0.4 nm (scale bar 18 μm). Vertical dashed lines in all panels indicate the detected T_N value. Error bars in (c), (d), (g), and (h) are indicated with vertical blue lines.

https://doi.org/10.1021/acs.nanolett.1c03010
Nano Lett. XXXX, XXX, XXX−XXX

$\gamma_{1,2}(T)$ can be attributed to the increasing contribution of thermoelastic dissipation to the nanomechanical motion of drums near phase transitions.[25]

To support the hypothesis that the temperature-dependent spectral changes are related to the temperature dependence of the dissipative terms in the equation of motion, we fabricated a sample of $MnPS_3$ that exhibits an antiferromagnetic to paramagnetic phase transition at $T_N \approx 78$ K.[27] In Figure 5e-h, we show the experimental data for $MnPS_3$ that revealed a behavior similar to $FePS_3$. As shown in Figure 5e, ω_2 softens near $T = 77$ K, which is close to T_N. We observe the splitting disappearing next to 75 ± 10 K, as displayed in Figure 5f. As expected, J does not show any systematic change near T_N, which is depicted in Figure 5g. However, in Figure 5h the cooperativity has a sharper drop in value as the sample goes from the strong to the weak coupling regime with increasing temperature. This coincides with a broad kink in $\gamma_{1,2}$ that is visible near the T_N value of $MnPS_3$, providing evidence for the hypothesis.

CONCLUSIONS

In conclusion, we have demonstrated a mechanism that mediates strong coupling between spatially separated membranes made of the antiferromagnetic materials $FePS_3$ and $MnPS_3$. This coupling mechanism can be switched on and tuned by an electrostatic gate. In addition, the electromechanical transfer of energy can be amplitude-modulated and is shown to be capable of performing bit-by-bit communication. This provides control advantages that can find use in the development of new device concepts, such as nanomechanical logic gates[7−9] and hybrid systems combining magnetic mechanical oscillators and qubits.[38] We have further shown that the magneto-mechanical properties of antiferromagnetic materials also can affect the coupling strength and cooperativity between the membranes next to the phase transition. For example, we have shown that the increasing mechanical dissipation[25] near the T_N values of $FePS_3$ and $MnPS_3$ diminishes the cooperativity of such coupled membrane systems as T approaches T_N. Therefore, coupled NEMS made of magnetic membrane resonators can provide a deeper insight into the coupling of magnetic properties with the nanomechanical motion. We also anticipate that in the future antiferromagnetic NEMS of this type can be useful to study more intricate magnetic phenomena, such as a magnetostriction in ultrathin layers[26] and the emission of spin currents by mechanical deformations—the piezospintronic effect.[39]

ASSOCIATED CONTENT

Supporting Information

The Supporting Information is available free of charge at https://pubs.acs.org/doi/10.1021/acs.nanolett.1c03010.

> Methods, continuum mechanics model of the circular membrane resonators of $FePS_3$, Joule dissipation model, linear coupled oscillators model, electromechanical coupling model, laser intensity and driving power dependence, laser position dependence, test sample without a microchannel connecting two suspended drums, finite element method simulations, reproducibility of measurements, and transfer of information (experimental details) (PDF)

AUTHOR INFORMATION

Corresponding Authors

Makars Šiškins − *Kavli Institute of Nanoscience, Delft University of Technology, 2628 CJ Delft, The Netherlands;* orcid.org/0000-0003-4295-2221; Email: m.siskins-1@tudelft.nl

Peter G. Steeneken − *Kavli Institute of Nanoscience, Delft University of Technology, 2628 CJ Delft, The Netherlands; Department of Precision and Microsystems Engineering, Delft University of Technology, 2628 CD Delft, The Netherlands;* Email: p.g.steeneken@tudelft.nl

Authors

Ekaterina Sokolovskaya − *Kavli Institute of Nanoscience, Delft University of Technology, 2628 CJ Delft, The Netherlands*

Martin Lee − *Kavli Institute of Nanoscience, Delft University of Technology, 2628 CJ Delft, The Netherlands;* orcid.org/0000-0003-1147-233X

Samuel Mañas-Valero − *Instituto de Ciencia Molecular (ICMol), Universitat de València, 46980 Paterna, Spain;* orcid.org/0000-0001-6319-9238

Dejan Davidovikj − *Kavli Institute of Nanoscience, Delft University of Technology, 2628 CJ Delft, The Netherlands;* orcid.org/0000-0002-6593-458X

Herre S. J. van der Zant − *Kavli Institute of Nanoscience, Delft University of Technology, 2628 CJ Delft, The Netherlands;* orcid.org/0000-0002-5385-0282

Complete contact information is available at: https://pubs.acs.org/10.1021/acs.nanolett.1c03010

Author Contributions

‖M.Š. and E.S. contributed equally to this work.

Author Contributions

M.Š., D.D., H.S.J.v.d.Z., and P.G.S. conceived the experiments. E.S. and M.Š. performed the laser interferometry measurements. M.L. and E.S. fabricated and inspected the samples. S.M.-V. synthesized and characterized the $FePS_3$ and $MnPS_3$ crystals. M.Š., E.S., and P.G.S. analyzed and modeled the experimental data. H.S.J.v.d.Z. and P.G.S. supervised the project. The paper was jointly written by all authors with a main contribution from M.Š. All authors discussed the results and commented on the paper.

Notes

The authors declare no competing financial interest.

ACKNOWLEDGMENTS

M.Š., M.L., H.S.J.v.d.Z., and P.G.S. acknowledge funding from the European Union's Horizon 2020 research and innovation program under grant agreement no. 881603. H.S.J.v.d.Z. and S.M.-V. thank COST Action MOLSPIN CA15128. S.M.-V. acknowledges financial support from the European Union (ERC AdG Mol-2D 788222), the Spanish MICINN (MAT2017-89993-R cofinanced by FEDER and Excellence Unit "Maria de Maeztu", CEX2019-000919-M), and the Generalitat Valenciana (Prometeo program and PO FEDER Program, ref IDIFEDER/2018/061 and IDIFEDER/2020/063). We thank E. Coronado and S. Lodha for useful discussions and feedback on the manuscript. The manuscript has associated numerical data in the Zenodo online data repository at 10.5281/zenodo.5750394.

■ REFERENCES

(1) Ekinci, K. L.; Roukes, M. L. Nanoelectromechanical Systems. *Rev. Sci. Instrum.* **2005**, *76*, 061101.
(2) Aspelmeyer, M.; Meystre, P.; Schwab, K. Quantum Optomechanics. *Phys. Today* **2012**, *65*, 29−35.
(3) Aspelmeyer, M.; Kippenberg, T. J.; Marquardt, F. Cavity Optomechanics. *Rev. Mod. Phys.* **2014**, *86*, 1391−1452.
(4) Spletzer, M.; Raman, A.; Sumali, H.; Sullivan, J. P. Highly Sensitive Mass Detection and Identification using Vibration Localization in Coupled Microcantilever Arrays. *Appl. Phys. Lett.* **2008**, *92*, 114102.
(5) Gil-Santos, E.; Ramos, D.; Jana, A.; Calleja, M.; Raman, A.; Tamayo, J. Mass Sensing Based on Deterministic and Stochastic Responses of Elastically Coupled Nanocantilevers. *Nano Lett.* **2009**, *9*, 4122−4127.
(6) Bannon, F.; Clark, J.; Nguyen, C.-C. High-Q HF Microelectromechanical Filters. *IEEE J. Solid-State Circuits* **2000**, *35*, 512−526.
(7) Tsai, C.-Y.; Kuo, W.-T.; Lin, C.-B.; Chen, T.-L. Design and Fabrication of MEMS Logic Gates. *J. Micromech. Microeng.* **2008**, *18*, 045001.
(8) Mahboob, I.; Yamaguchi, H. Bit Storage and Bit Flip Operations in an Electromechanical Oscillator. *Nat. Nanotechnol.* **2008**, *3*, 275−279.
(9) Masmanidis, S. C.; Karabalin, R. B.; Vlaminck, I. D.; Borghs, G.; Freeman, M. R.; Roukes, M. L. Multifunctional Nanomechanical Systems via Tunably Coupled Piezoelectric Actuation. *Science* **2007**, *317*, 780−783.
(10) Karabalin, R. B.; Lifshitz, R.; Cross, M. C.; Matheny, M. H.; Masmanidis, S. C.; Roukes, M. L. Signal Amplification by Sensitive Control of Bifurcation Topology. *Phys. Rev. Lett.* **2011**, *106*, 094−102.
(11) Okamoto, H.; Gourgout, A.; Chang, C.-Y.; Onomitsu, K.; Mahboob, I.; Chang, E. Y.; Yamaguchi, H. Coherent Phonon Manipulation in Coupled Mechanical Resonators. *Nat. Phys.* **2013**, *9*, 480−484.
(12) Faust, T.; Rieger, J.; Seitner, M. J.; Kotthaus, J. P.; Weig, E. M. Coherent Control of a Classical Nanomechanical Two-Level System. *Nat. Phys.* **2013**, *9*, 485−488.
(13) Zhu, D.; Wang, X.-H.; Kong, W.-C.; Deng, G.-W.; Wang, J.-T.; Li, H.-O.; Cao, G.; Xiao, M.; Jiang, K.-L.; Dai, X.-C.; Guo, G.-C.; Nori, F.; Guo, G.-P. Coherent Phonon Rabi Oscillations with a High-Frequency Carbon Nanotube Phonon Cavity. *Nano Lett.* **2017**, *17*, 915−921.
(14) Shim, S.-B.; Imboden, M.; Mohanty, P. Synchronized Oscillation in Coupled Nanomechanical Oscillators. *Science* **2007**, *316*, 95−99.
(15) Chen, C.; Rosenblatt, S.; Bolotin, K. I.; Kalb, W.; Kim, P.; Kymissis, I.; Stormer, H. L.; Heinz, T. F.; Hone, J. Performance of Monolayer Graphene Nanomechanical Resonators with Electrical Readout. *Nat. Nanotechnol.* **2009**, *4*, 861−867.
(16) Chen, C.; Lee, S.; Deshpande, V. V.; Lee, G.-H.; Lekas, M.; Shepard, K.; Hone, J. Graphene Mechanical Oscillators with Tunable Frequency. *Nat. Nanotechnol.* **2013**, *8*, 923−927.
(17) Lemme, M. C.; Wagner, S.; Lee, K.; Fan, X.; Verbiest, G. J.; Wittmann, S.; Lukas, S.; Dolleman, R. J.; Niklaus, F.; van der Zant, H. S. J.; Duesberg, G. S.; Steeneken, P. G. Nanoelectromechanical Sensors Based on Suspended 2D Materials. *Research* **2020**, *2020*, 1−25.
(18) Novoselov, K. S.; Mishchenko, A.; Carvalho, A.; Neto, A. H. C. 2D materials and van der Waals Heterostructures. *Science* **2016**, *353*, 6298.
(19) Mathew, J. P.; Patel, R. N.; Borah, A.; Vijay, R.; Deshmukh, M. M. Dynamical Strong Coupling and Parametric Amplification of Mechanical Modes of Graphene Drums. *Nat. Nanotechnol.* **2016**, *11*, 747−751.
(20) Liu, C.-H.; Kim, I. S.; Lauhon, L. J. Optical Control of Mechanical Mode-Coupling within a MoS_2 Resonator in the Strong-Coupling Regime. *Nano Lett.* **2015**, *15*, 6727−6731.
(21) Prasad, P.; Arora, N.; Naik, A. K. Gate Tunable Cooperativity between Vibrational Modes. *Nano Lett.* **2019**, *19*, 5862−5867.
(22) Keşkekler, A.; Shoshani, O.; Lee, M.; van der Zant, H. S. J.; Steeneken, P. G.; Alijani, F. Tuning Nonlinear Damping in Graphene Nanoresonators by Parametric−Direct Internal Resonance. *Nat. Commun.* **2021**, *12*, 1099.
(23) Luo, G.; Zhang, Z.-Z.; Deng, G.-W.; Li, H.-O.; Cao, G.; Xiao, M.; Guo, G.-C.; Tian, L.; Guo, G.-P. Strong Indirect Coupling between Graphene-Based Mechanical Resonators via a Phonon Cavity. *Nat. Commun.* **2018**, *9*, 383.
(24) Zhang, Z.-Z.; Song, X.-X.; Luo, G.; Su, Z.-J.; Wang, K.-L.; Cao, G.; Li, H.-O.; Xiao, M.; Guo, G.-C.; Tian, L.; Deng, G.-W.; Guo, G.-P. Coherent Phonon Dynamics in Spatially Separated Graphene Mechanical Resonators. *Proc. Natl. Acad. Sci. U. S. A.* **2020**, *117*, 5582−5587.
(25) Šiškins, M.; Lee, M.; Mañas-Valero, S.; Coronado, E.; Blanter, Y. M.; van der Zant, H. S. J.; Steeneken, P. G. Magnetic and Electronic Phase Transitions Probed by Nanomechanical Resonators. *Nat. Commun.* **2020**, *11*, 2698.
(26) Jiang, S.; Xie, H.; Shan, J.; Mak, K. F. Exchange Magnetostriction in Two-Dimensional Antiferromagnets. *Nat. Mater.* **2020**, *19*, 1295−1299.
(27) Takano, Y.; Arai, N.; Arai, A.; Takahashi, Y.; Takase, K.; Sekizawa, K. Magnetic Properties and Specific Heat of MPS_3 (M = Mn, Fe, Zn). *J. Magn. Magn. Mater.* **2004**, *272−276*, E593−E595.
(28) Lee, J.-U.; Lee, S.; Ryoo, J. H.; Kang, S.; Kim, T. Y.; Kim, P.; Park, C.-H.; Park, J.-G.; Cheong, H. Ising-Type Magnetic Ordering in Atomically Thin $FePS_3$. *Nano Lett.* **2016**, *16*, 7433−7438.
(29) Davidovikj, D.; Scheepers, P. H.; van der Zant, H. S. J.; Steeneken, P. G. Static Capacitive Pressure Sensing Using a Single Graphene Drum. *ACS Appl. Mater. Interfaces* **2017**, *9*, 43205−43210.
(30) Chen, C. Graphene Nanoelectromechanical Resonators and Oscillators; Ph.D. thesis, Columbia University, 2013.
(31) Weber, P.; Güttinger, J.; Tsioutsios, I.; Chang, D. E.; Bachtold, A. Coupling Graphene Mechanical Resonators to Superconducting Microwave Cavities. *Nano Lett.* **2014**, *14*, 2854−2860.
(32) Song, X.; Oksanen, M.; Sillanpää, M. A.; Craighead, H. G.; Parpia, J. M.; Hakonen, P. J. Stamp Transferred Suspended Graphene Mechanical Resonators for Radio Frequency Electrical Readout. *Nano Lett.* **2012**, *12*, 198−202.
(33) Will, M.; Hamer, M.; Müller, M.; Noury, A.; Weber, P.; Bachtold, A.; Gorbachev, R. V.; Stampfer, C.; Güttinger, J. High Quality Factor Graphene-Based Two-Dimensional Heterostructure Mechanical Resonator. *Nano Lett.* **2017**, *17*, 5950−5955.
(34) Morell, N.; Reserbat-Plantey, A.; Tsioutsios, I.; Schädler, K. G.; Dubin, F.; Koppens, F. H. L.; Bachtold, A. High Quality Factor Mechanical Resonators Based on WSe_2 Monolayers. *Nano Lett.* **2016**, *16*, 5102−5108.
(35) Zanette, D. H. Energy Exchange between Coupled Mechanical Oscillators: Linear Regimes. *J. Phys. Commun.* **2018**, *2*, 095015.
(36) Haines, C.; Coak, M.; Wildes, A.; Lampronti, G.; Liu, C.; Nahai-Williamson, P.; Hamidov, H.; Daisenberger, D.; Saxena, S. Pressure-Induced Electronic and Structural Phase Evolution in the van der Waals Compound $FePS_3$. *Phys. Rev. Lett.* **2018**, *121*, 266801.
(37) Evarestov, R. A.; Kuzmin, A. Origin of Pressure-Induced Insulator-to-Metal Transition in the van der Waals Compound $FePS_3$ from First-Principles Calculations. *J. Comput. Chem.* **2020**, *41*, 1337−1344.
(38) Lee, D.; Lee, K. W.; Cady, J. V.; Ovartchaiyapong, P.; Jayich, A. C. B. Topical Review: Spins and Mechanics in Diamond. *J. Opt.* **2017**, *19*, 033001.
(39) Ulloa, C.; Troncoso, R. E.; Bender, S. A.; Duine, R. A.; Nunez, A. S. Piezospintronic Effect in Honeycomb Antiferromagnets. *Phys. Rev. B: Condens. Matter Mater. Phys.* **2017**, *96*, 104419.

https://doi.org/10.1021/acs.nanolett.1c03010
Nano Lett. XXXX, XXX, XXX−XXX